Section 2

Data sets, diagnostic and dynamical investigations, statistical post-processing , multi-year reanalyses and associated studies

Variability of global SLP fields of pressure according to NCEP/NCAR reanalysis

M.G. Akperov
A.M. Obukhov Institute of Atmospheric Physics RAS, Moscow, Russia
aseid@ifaran.ru

Interannual variability of a global field of a sea level pressure (SLP) P by data from reanalysis is analyzed.

Figure 1 shows the distribution of the SLP standard interannual deviations δP from NCEP/NCAR reanalysis (Kistler et al., 2001).

Significant variations of the δP are noted over oceans in high and middle latitudes during winter. Large δP values changes are associated with the centers of action in the atmosphere. Extreme δP values are associated with the oceanic centers of action in high latitudes of the Northern Hemisphere.

Figure 2 shows differences of the δP between two periods (1987-2006 and 1948-1967). Large changes are noted for high latitudes in both hemispheres. Decrease of the δP has been noted for the Antarctic and Greenland region, in midlatitude of the Pacific Ocean, the coast of Greenland and Pacific Ocean. Increase of the δP has been noted for the central part of East European plain of Russia.

This work is supported by the Russian Foundation for Basic Research and by the programs of the Russian Academy of Sciences.

References

Kistler R., Kalnay E., Collins W., et al. The NCEP 50-year reanalysis: monthly means CD-ROM and documentation. Bull. Amer. Met. Soc. 2001. V82. P.247-266.

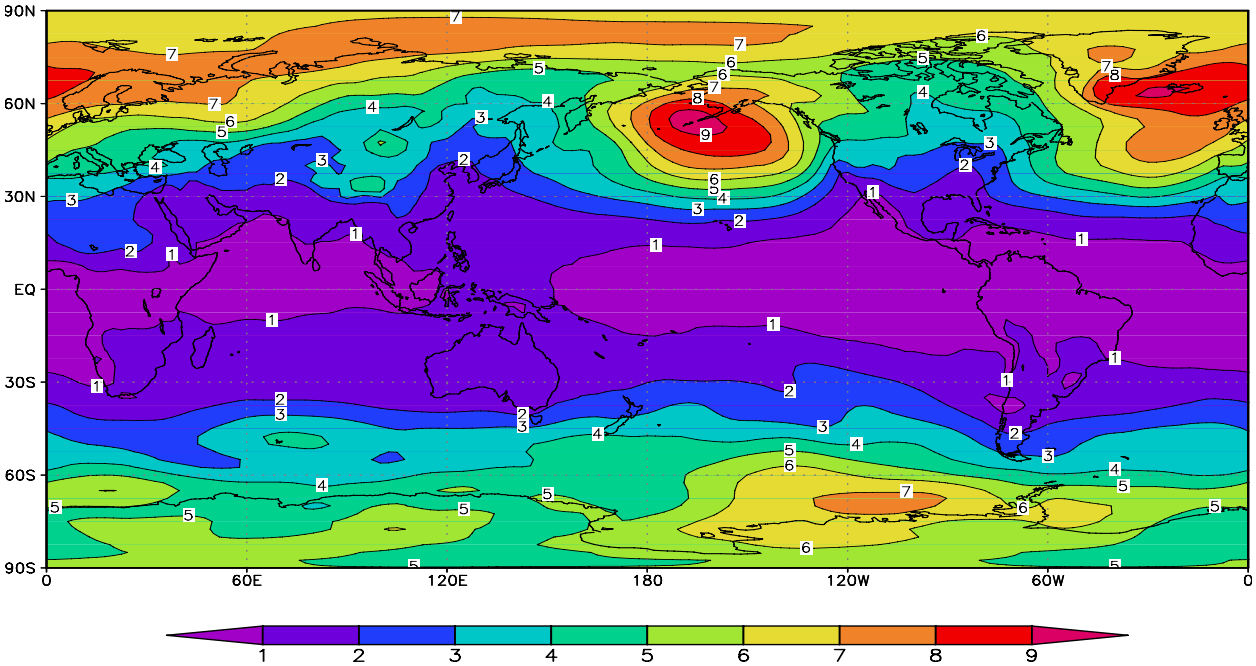

Fig. 1. Spatial distribution of the standard interannual deviation δP (SD) of the SLP in winter (a) from NCEP/NCAR reanalysis for the period 1948-2006.

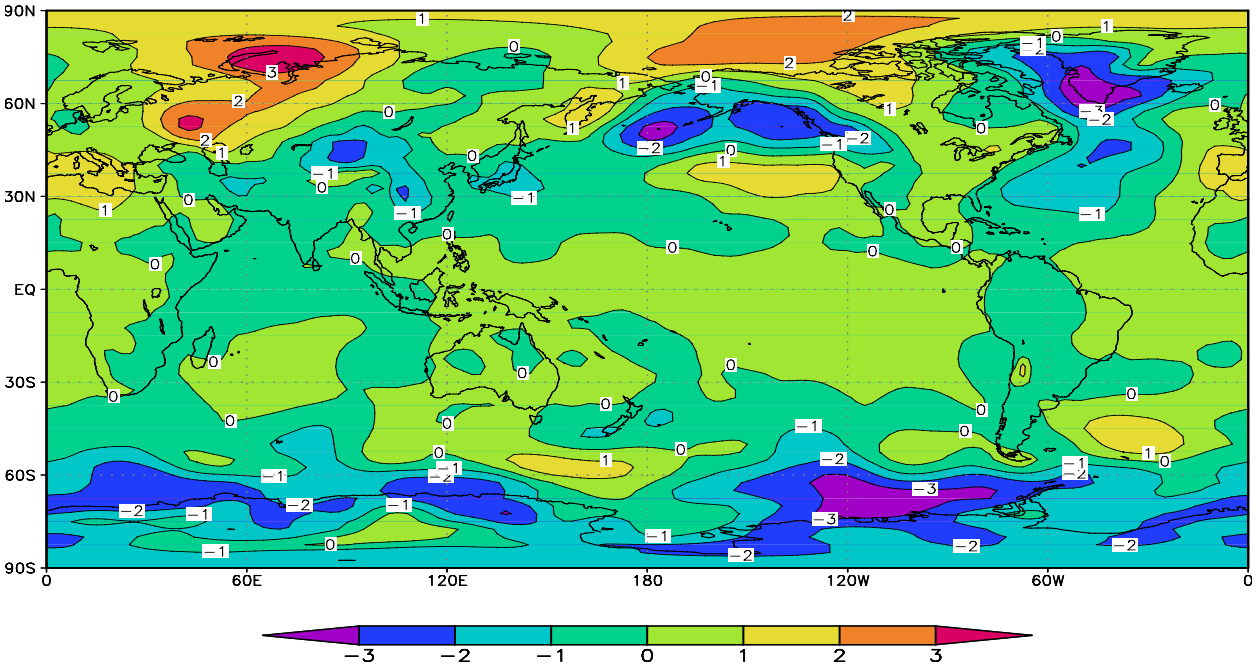

Fig. 2. Spatial distribution of the differences SD between two periods (1987-2006 and 1948-1967) (b) from NCEP/NCAR reanalysis for winter.

Temperature Trends in Troposphere over North-West of Siberia Detected by the Method Based on the Using of Hourly Observations

Oleg A. Alduchov and Irina V. Chernykh

Russian Institute of Hydrometeorological Information – Word Data Center, Obninsk, Russia,
E-mail: aoa@meteo.ru, civ@meteo.ru

Radiosonde sounding data from dataset CARDS [Eskridge et al, 1995] for two stations: coastal station Ostrov Dikson and continental station Salehard, placed in North-West of Siberia were used for research of climatic changes of temperature (T) at the standard isobaric levels in Arctic troposphere over period 1964-10.2007 years.

Distribution of observations number used for researches for standard isobaric levels is different for different months due different height of sound rising and different historical request for reporting of sounding results. (For example, data for 1000 hPa and 925 hPa are including in aerological telegram after 1967 year.) Number of observations for 00 GMT and 12 GMT is practically the same for both stations. Partly estimations of trends are dependent from quality data. For example, numbers of observations before and after running of complex quality control procedure [Alduchov and Eskridge, 1996] are presented in tables 1 and 2 for different months, seasons and year for level 850 hPa. Number of rejected observations foot up to 1.1% (Ostrov Dikson) and 1.4% (Salehard) from all soundings (table 2 for year).

TABLE 1. Number of T observations before and after complex quality control for level 850 hPa for different months.

Station	Jan.	Feb.	Mar.	Apr.	May	Jun.	Jul.	Aug.	Sep.	Oct.	Nov.	Dec.
Ostrov Dikson	1975 1961	1836 1822	2068 2050	1937 1915	2065 2035	1971 1944	2031 2009	1849 1832	1835 1817	1911 1889	1936 1911	1987 1966
Salehard	2347 2325	2139 2120	2440 2409	2411 2398	2384 2334	2269 2216	2158 2129	2238 2204	2267 2239	2274 2244	2106 2083	2250 2210

TABLE 2. The same as TABLE 1 for seasons and for year.

Station		Winter	Spring	Summer	Autumn	Year	Year (%)
Ostrov Dikson	Before control After control	5798 5749	6070 6000	5851 5785	5682 5617	23401 23151	100 98.9
Salehard	Before control After control	6736 6655	7235 7141	6665 6549	6647 6566	27283 26911	100 98.6

The multiannual monthly means of temperature are presented for different months, seasons and for year at figure 1a. Corresponding linear trends in time series of temperature anomalies at the standard isobaric levels in troposphere, calculated by the method based on the using of hourly observations with taking into account the possible time correlations of observations [Alduchov and Chernykh, 2008], are presented at figure 1b-1d. Due continuity of climatic changes in atmosphere all detected trends (with different significance), trends with significance not less than 50% and trends with significance not less than 95% are presented at the figure 1b, 1c, 1d correspondently.

Figure 1b shows that climatic changes in Arctic troposphere are inhomogeneous in time and space. Warming is detected at all levels in troposphere over Salehard for all months (with exception December), seasons and year in total. Over Ostrov Dikson warming is detected for all months, seasons and year only in low troposphere. Only for March, May and July warming is detected for middle and high troposphere too. Cooling is detected in middle and/or high troposphere for other mounths, for winter, summer and autumn. Small cooling was detected in high levels of troposphere for year in total. Figure 1c shows that not all determined trends were detected with significance more than 50% for both stations.

Figure 1d shows that warming with significance not less than 95% was detected only for January, May and June, spring, summer and autumn and year for both stations. But the warming was detected at most levels of troposphere over Salehard and only in low troposphere over Ostrov Dikson.

Linear trends values for temperature anomalies for levels 850 hPa, 700 hPa and 500 hPa are presented in Table 3 for January, May, June and year. Largest warming for both stations was detected at level 850 hPa. For Ostrov Dikson it was detected for January with decadal changes 0.97ºC/Dec. For Salehard it was detected for June with decadal changes 0.90ºC/Dec. For year largest warming was detected at level 850 hPa for Ostrov Dikson and for Salehard with decadal changes 0.36ºC/Dec. and 0.38 ºC/Dec. correspondently.

The results can be used for modeling of climate change.

Acknowledgment. Study was partly supported by Russian Basic Research Foundation (RBRF), project 07-05-00264 and IPY project CLOMAP.

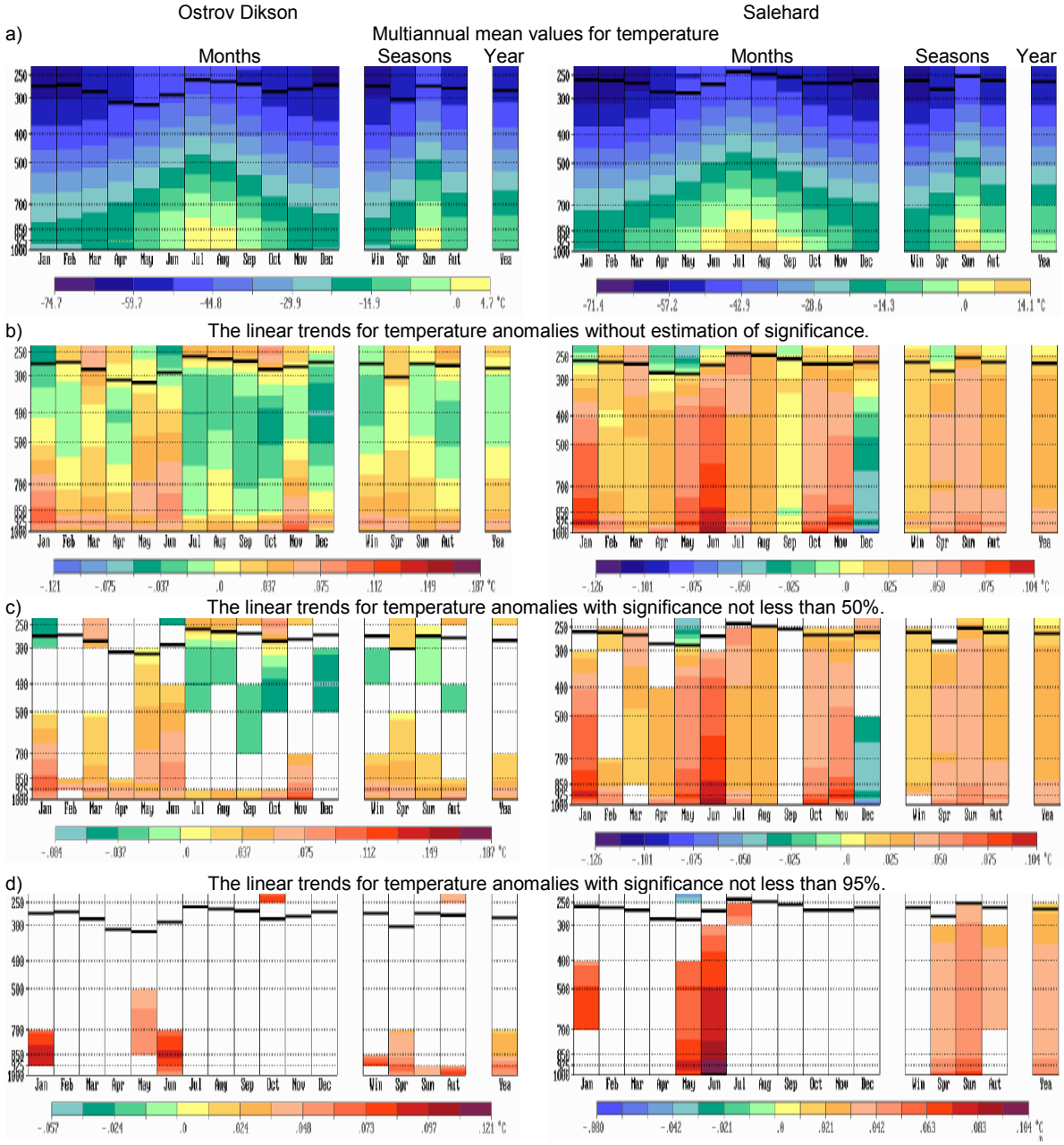

Fig. 1. Multiannual mean values for temperature (a) and linear trends for temperature anomalies (ºC/Year) for the isobaric levels calculated on the base of hourly observations with taking into account the time correlations of observations for different months (in the left), seasons (in the center) and for year (in the right) without estimation of significance (b), with significance not less than 50% (c) and 95% (d). The first tropopause is marked by black line. Stations: Ostrov Dikson (left column) and Salehard (right column). CARDS. 1964 – 10.2007.

TABLE 3. Linear trends for temperature anomalies (ºC/Decade) for standard isobaric levels 850 hPa, 700 hPa, 500 hPa calculated on the base of hourly observations with taking into account the time correlations of observations, for January, May, June and year. Trends with significance 99% are marked by Italic. Significance of other trend is not less than 93%.

Station	January			May			June			Year		
	Standard isobaric levels, hPa											
	500	**700**	**850**	**500**	**700**	**850**	**500**	**700**	**850**	**500**	**700**	**850**
Ostrov Dikson	-	.69	*.97*	.40	*.58*	*.59*	.46	.69	*.89*	-	.22	*.36*
Salehard	.64	.72	.79	*.63*	*.59*	*.69*	*.73*	*.78*	*.90*	*.36*	*.35*	*.38*

REFERENCES

Alduchov O.A., Chernykh I.V. About changes of temperature-humidity regime in troposphere over Antarctic Peninsula // Proc. RIHMI-WDC. 2008, 173, 270-294.

Alduchov O.A., Eskridge R.E. Complex quality control of upper air parameters at mandatory and significant levels for the CARDS dataset. NCDC Report. 1996. 151pp.

Eskridge R.E., Alduchov O.A., Chernykh I.V., Zhai P., Doty S.R., Polansky A.C. A Comprehensive Aerological Reference Data Set (CARDS): Rough and systematic errors // Bull. Amer. Meteor. Soc. 1995, **76**, 1959-1775.

Water Vapour Amount Trends in Troposphere over North-West of Siberia Detected by the Method Based on the Using of Hourly Observations

Oleg A. Alduchov and Irina V. Chernykh

Russian Institute of Hydrometeorological Information – Word Data Center, Obninsk, Russia,
E-mail: aoa@meteo.ru, civ@meteo.ru

Estimations of climatic changes for water vapour amount (VA) for standard isobaric levels in troposphere over North-West of Siberia are presented for stations Ostrov Dixon and Salehard on base dataset CARDS [Eskridge et al, 1995] over period 1964-10.2007 years.

Number of humidity observations used for researches have shown in Table 1 for different months for standard levels: 850 hPa, 700 hPa, 500 hPa and 400 hPa. Table 1 demonstrates that number of humidity observations is decreasing with height, especially in cold months.

TABLE 1. Number of humidity observations used for researches for different levels for different month.

Level (hPa)	Jan.	Feb.	Mar.	Apr.	May	Jun.	Jul.	Aug.	Sep.	Oct.	Nov.	Dec.
	Ostrov Dixon											
400	654	675	816	747	1013	1275	1420	1193	1028	684	655	644
500	952	981	1203	1238	1486	1377	1451	1253	1256	1158	1079	1023
700	1399	1341	1523	1445	1504	1392	1464	1267	1274	1274	1357	1380
850	1406	1343	1528	1447	1506	1394	1468	1267	1277	1283	1361	1388
	Salehard											
400	1547	1391	1657	1716	1758	1801	1711	1731	1789	1639	1429	1489
500	1813	1658	1985	1970	1885	1843	1733	1762	1864	1639	1670	1755
700	1926	1748	2041	2022	1913	1845	1742	1795	1894	1881	1756	1870
850	1902	1729	1995	1987	1877	1803	1693	1762	1872	1854	1736	1842

The multiannual monthly mean values for VA for isobaric levels and linear trends in correspondent time series for VA anomalies, calculated on the base of hourly observations with taking into account the time correlations of observations [Alduchov et al, 2006, Alduchov and Chernykh, 2008] are presented at Figure 1. The trends are presented for different months, seasons and for year without estimation of significance, with significance not less than 50% and 95%.

Figure 1a demonstrates that biggest mean values of VA in troposphere over both stations take place in summer. For 500 hPa it equal to 13.7 kg/m^2 for Ostrov Dikson and 18.1 kg/m^2 - for Salehard. But tendencies of climatic changes of VA for summer are opposite direction for the stations. VA is decreasing over Ostrov Dikson and is increasing over Salehard (fig. 1b, 1c). For example, trends of VA for 500 hPa, detected with significance 82% and 92%, equal to -0.2 kg/m^2/dec. and 0.3 kg/m^2/dec. correspondently.

Figure 1d shows that trends with significance not less than 95% are detected only in high troposphere over Ostrov Dikson for October (for 400 hPa trend equal to 1.2 kg/m^2/dec.) and in low troposphere over Salehard for June, summer and year (for 700 hPa decadal changes equal to 0.5 kg/m^2/dec., 0.3 kg/m^2/dec. and 0.1 kg/m^2/dec. correspondently).

It was shown in [1] that warming with significance not less than 95% was detected only for January, May and June, spring, summer and autumn and year for both stations. In Table 2 linear trends values for VA anomalies and its significance are presented for these months and year. According [1] and Table 2 the warming and increasing VA for these months and year are detected at most levels of troposphere over Salehard and only in low troposphere over Ostrov Dikson.

TABLE 2. Linear trends for vapour amount VA anomalies (kg/m^2/dec) for standard isobaric levels 850 hPa, 700 hPa, 500 hPa calculated on the base of hourly observations with taking into account the time correlations of observations, for January, May, June and year and its significance (%).

Station		January			May			June			Year		
		Standard isobaric levels, hPa											
		500	700	850	500	700	850	500	700	850	500	700	850
Ostrov Dikson	Trend	.37	.09	.08	-	-	.05	-	.13	.13	-	-	.05
	Significance	99	67	85			56		54	79			88
Salehard	Trend	.18	.14	.08	.16	.16	.12	.61	.53	.35	.13	.12	.10
	Significance	84	80	77	59	69	77	94	96	97	92	96	99

The results can be used for analysis of climate change of humidity in Arctic atmosphere.

Acknowledgment. Study was supported by Russian Basic Research Foundation (RBRF), project 07-05-00264 and IPY project CLOMAP.

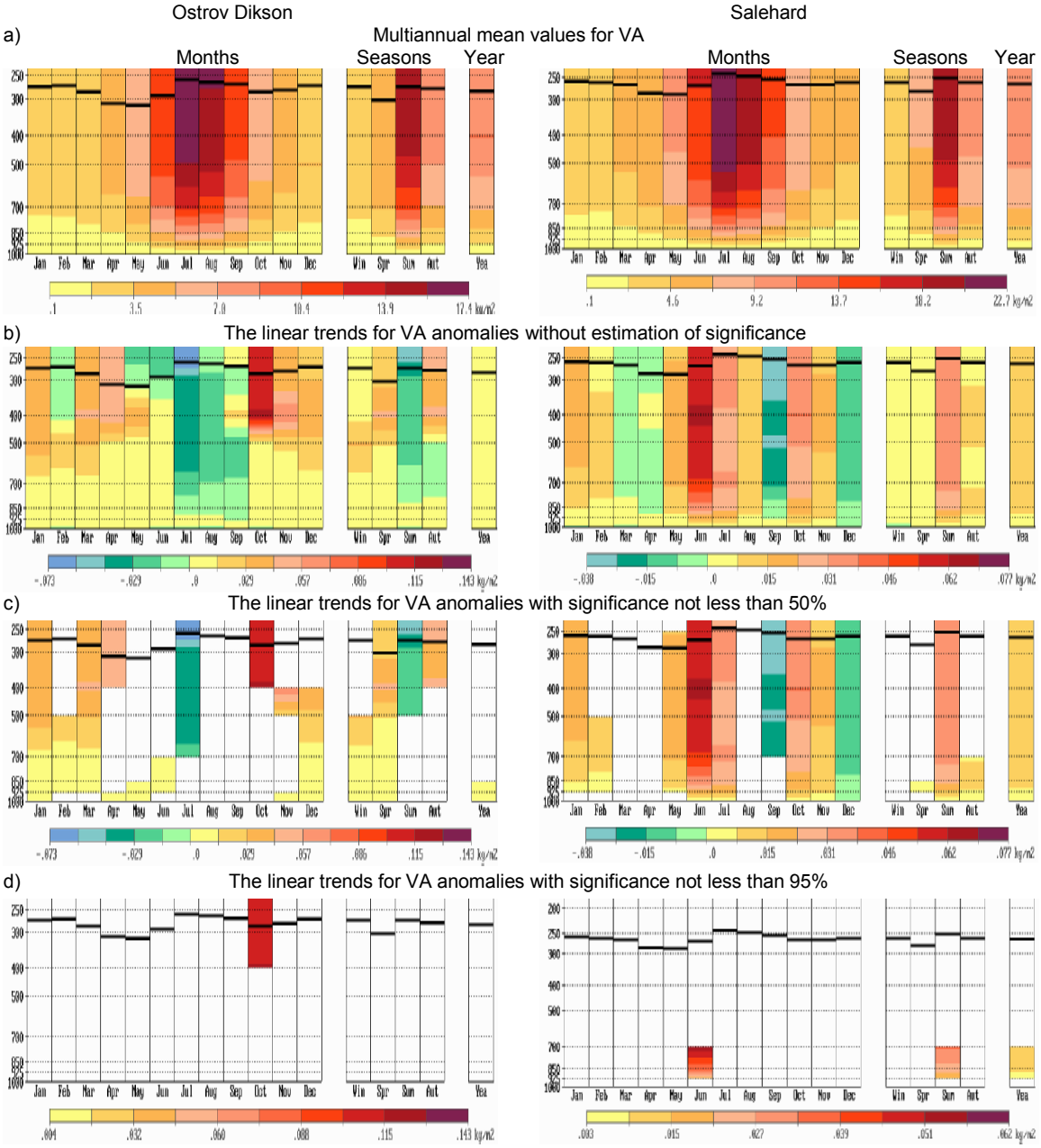

Fig. 1. Multiannual mean values (kg/m^2) for vapour amount VA and linear trends in time series of vapour amount anomalies (kg/m^2/year) for the isobaric levels calculated on the base of hourly observations with taking into account the time correlations of observations for different months (in the left), seasons (in the center) and for year (in the right) without estimation of significance, with significance not less than 50% and 95%. The first tropopause is marked by black line. Stations Ostrov Dikson (left column) and Salehard (right column). CARDS. 01.1964 – 10.2007.

REFERENCES

Alduchov O.A., Chernykh I.V. Temperature Trends in Troposphere over North-West of Siberia Detected by the Method Based on the Using of Hourly Observations. Research Activities in Atmospheric and Oceanic Modelling. WMO. Geneva 2. Switzerland. http://collaboration.cmc.ec.gc.ca/science/wgne/BlueBook/ 2008.

Alduchov O.A., Chernykh I.V. About changes of temperature-humidity regime in troposphere over Antarctic peninsula. Alduchov O.A., Chernykh I.V. About changes of temperature-humidity regime in troposphere over Antarctic Peninsula // Proc. RIHMI-WDC. 2008, 173, 270-294.

Alduchov O.A., Lagun V. E., Chernykh I.V., Jagovkina S.V. About climatic changes of troposphere over Antarctic peninsula. - "Problemy Klimatologi Polarnej". 2006. **16.** 7-22.

Eskridge R.E., Alduchov O.A., Chernykh I.V., Zhai P., Doty S.R., Polansky A.C. A Comprehensive Aerological Reference Data Set (CARDS): Rough and systematic errors // Bull. Amer. Meteor. Soc. 1995, **76**, 1959-1775.

Total cloudiness changes during 1983-2006 from ISCCP data

A.V. Chernokulsky
A.M. Obukhov Institute of Atmospheric Physics RAS, Moscow, Russia
chern_av@ifaran.ru

Clouds play an important role in regulating the flow of radiation at the top of the atmosphere and at the surface (IPCC, 2007). The response of cloudiness to increasing greenhouse gases and temperature represents one of the largest uncertainties in climate model predictions.

Changes in total cloudiness from ISCCP data (Rossow and Duenas, 2004) in last two decades were estimated. D2 product, which correspond monthly averaged values on grid 2,5°x2,5° and cover time period from July 1983 to June 2006 was used.

According to this data, total cloudiness decreases from the middle eighties to the end of previous century (Fig. 1) (Mokhov and Chernokulsky 2003; Chernokulsky and Mokhov, 2006, Chernokulsky 2007). Global averaged cloudiness trend n from 1987 to 2000 is equal to -0.0027 yr^{-1} (corresponding coefficient of correlation r amount -0.96). But since 2001 cloudiness began to growth (n = 0,0005 yr^{-1}, r = 0.3) so finally n for all period is equal to -0.0017 yr^{-1} (r = -0.88).

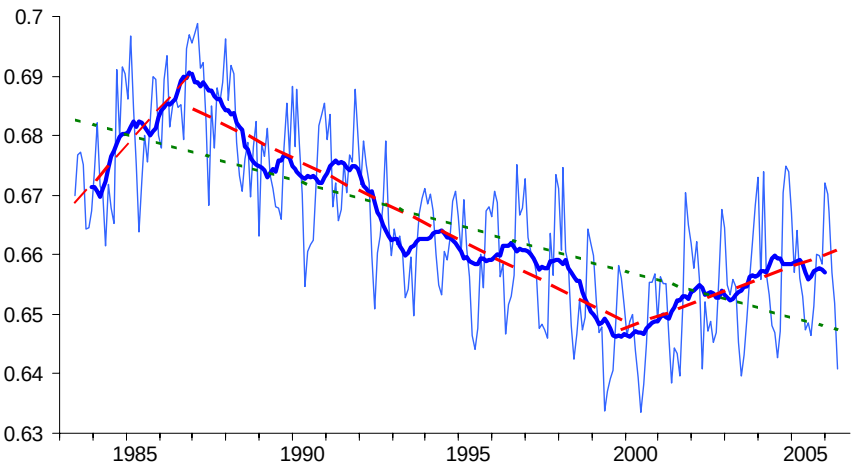

Fig.1 Global averaged cloudiness changes from July 1983 to June 2006 (blue curve), its 12 month moving average (blue thick curve), trend-line for all period (green short-dashed line), and trend-lines for period with cloudiness rise and decrease (red long-dashed line)

The same tendencies take place not only in global mean, but also in regional scale (tropic and midlatitude in both hemisphere) and both for ocean and for land surface (Table1). Cloudiness maximums for all regions note at period between 1985 and 1988 years, with only one exception (for land in southern hemisphere's midlatitude it is 1992). Cloudiness minimums note at 1998-2002 years, except land in southern tropical zone (1994) and southern midlatitude zone (1993 for ocean and 1996 for land).

The highest modulo of n observed in northern hemisphere tropical zone beneath ocean surface (n =-0.0031, r = -0.85). The lowest modulo n obtained in southern midlatitude zone beneath ocean surface (n =-0.0004, r = -0.44). In addition, total cloudiness here has a highest value (0.83). The lowest value observed beneath land in northern tropical zone (0.5), and global mean cloudiness equal 0.67.

This work was partly supported by the Russian Foundation for Basic Research, by the Programs of the Russian Academy of Sciences and by the Russian President scientific grant.

Table 1. Statistical characteristic of total cloudiness in different region

Region			mean	max	min	Trend (n)+ STD (yr^{-1})	r
Global	NH+SH (90S-90N)	Ocean+Land	0.67	0.69 (1987)	0.65 (2000)	-0.0017±0.0002	-0.88
		Ocean	0.70	0.73 (1986)	0.68 (2000)	-0.0018±0.0002	-0.86
		Land	0.57	0.59 (1987)	0.55 (2002)	-0.0014±0.0002	-0.86
	NH (EQ-90N)	Ocean+Land	0.64	0.67 (1987)	0.62 (2000)	-0.0019±0.0003	-0.86
		Ocean	0.68	0.71 (1986)	0.66 (1998)	-0.0023±0.0003	-0.86
		Land	0.58	0.61 (1987)	0.56 (2000)	-0.0014±0.0003	-0.77
	SH (90S-EQ)	Ocean+Land	0.69	0.71 (1987)	0.67 (1999)	-0.0014±0.0002	-0.85
		Ocean	0.72	0.74 (1987)	0.70 (1999)	-0.0014±0.0002	-0.79
		Land	0.54	0.56 (1986)	0.51 (2002)	-0.0016±0.0003	-0.75
Tropical zone	NH+SH (30S-30N)	Ocean+Land	0.60	0.63 (1985)	0.57 (2000)	-0.0026±0.0003	-0.89
		Ocean	0.62	0.66 (1985)	0.59 (2000)	-0.0028±0.0003	-0.88
		Land	0.52	0.55 (1988)	0.50 (2001)	-0.0020±0.0003	-0.85
	NH (EQ-30N)	Ocean+Land	0.59	0.62 (1986)	0.56 (2000)	-0.0028±0.0004	-0.86
		Ocean	0.62	0.66 (1985)	0.59 (1998)	-0.0031±0.0004	-0.85
		Land	0.50	0.53 (1988)	0.46 (2000)	-0.0021±0.0004	-0.73
	SH (30S-EQ)	Ocean+Land	0.60	0.63 (1985)	0.58 (1999)	-0.0024±0.0003	-0.88
		Ocean	0.62	0.65 (1987)	0.59 (1999)	-0.0026±0.0004	-0.84
		Land	0.55	0.58 (1986)	0.53 (1994)	-0.0019±0.0003	-0.81
Mid-latitude zone	NH (30N -60N)	Ocean+Land	0.69	0.72 (1987)	0.67 (2000)	-0.0015±0.0003	-0.77
		Ocean	0.77	0.80 (1986)	0.75 (2000)	-0.0018±0.0003	-0.81
		Land	0.60	0.63 (1987)	0.58 (2000)	-0.0012±0.0003	-0.66
	SH (60S-30S)	Ocean+Land	0.81	0.83 (1986)	0.80 (1993)	-0.0004±0.0002	-0.45
		Ocean	0.83	0.84 (1986)	0.82 (1993)	-0.0004±0.0002	-0.44
		Land	0.55	0.58 (1992)	0.53 (1996)	-0.0006±0.0004	-0.30

References

Chernokulsky A.V. Cloudiness anomalies and El Nino effects. Research Activities in Atmospheric and Oceanic Modelling. J. Cote (ed.). 2007 WMO/TD-No.1397, 02.05-02.06

Chernokulsky A.V., Mokhov I.I. Global and Regional Cloudiness Changes by Satellite Data:Relationship with Temperature and El Nino Effects. Research Activities in Atmospheric and Oceanic Modelling. J. Cote (ed.). 2006. WMO/TD-No.1347, 02.09-02.10

Climate Change 2007: The Physical Science Basis. Contribution of Working Group I to the Fourth Assessment Report of the Intergovernmental Panel on Climate Change, Ed by Solomon S., *et al.* Cambridge University Press, Cambridge, 2007.

Mokhov I.I., Chernokulsky A.V. Global cloudiness: Tendencies of Change from ISCCP data. Research Activities in Atmospheric and Oceanic Modelling. J. Cote (ed.). 2003. WMO/TD-No.1161, 02.07-02.08.

Rossow, W.B., and E. Duenas. The International Satellite Cloud Climatology Project(ISCCP) web site: An online resource for research. *Bull. Amer. Meteorol. Soc.*2004, 85, 167-172.

Ice Core Isotope Inversion for Determining Global Climate Indices

Scott Gregory, David Noone, and David Schneider

Department of Atmospheric and Oceanic Sciences and Cooperative Institute for Research in the Environmental Sciences, University of Colorado, Boulder, Colorado, USA

(email: scott.gregory@colorado.edu)

The history of climate variability is not well simulated by climate models, however proxy climate records offer additional constraints for developing atmospheric analyses that to date have not been included in constructing gridded fields to represent the history of atmospheric circulation statistics. The isotopic composition of snow, captured by ice cores, is a useful proxy to consider since the physics controlling the isotopic composition is well known and can be modeled in atmospheric circulation models. Thus, we suggest model estimates of the linkage between the ice core records and the atmospheric circulation can be used in an inverse sense to estimate the atmospheric variability.

Climate models that include stable water isotopes have been run for simulation of the 1870-2003 climate by the Stable Water Isotope Intercomparison Group (SWING). An array of 35 ice cores is distributed at many latitudes and they act as long proxy records for features of global climate such as the global temperature, El Nino Southern Oscillation, Southern Annular Mode, North Pacific Index, and North Atlantic Oscillation. These indices may be constructed from the SWING models, since they are generally represented by pressure differences between stations. The ice core records may also be derived from the SWING models by determining the net isotopic deposition at each core site. Direct measurements and/or reconstructions of the climate indices have been performed for the 20th century, and thus we have both fully empirical and fully model databases of the ice cores' response to shifts in such climate features.

The inverse approach for estimating climate indices from isotope records is characterized by the forward model:

$$y = Kx + \varepsilon \qquad \text{(Rodgers, 2000)}$$

where y is the array of isotope records, x is the array of climate indices, K is the weighting function matrix, and ε is the error. The weighting function matrix, K, characterizes the sensitivity of the ice cores to the climate indices, the sensitivity of the i^{th} ice core to the j^{th} climate index is:

$$k_{ij} = \frac{\partial y_i}{\partial x_j}$$

The resulting K matrix is of dimensions m x n, where m is the number of ice cores and n is the number of climate indices. A K matrix for the relationship between the ice cores and climate indices is constructed by performing a multiple regression analysis for each ice core:

$$y_i = k_{11}x_1 + k_{12}x_2 + \ldots k_{1j}x_j + \varepsilon_i$$

where the ks are the multiple regression coefficients, and ε is the residual of the regression and is the estimated error.

Initial steps in developing the methodology were to use only SWING model outputs to test the ability of the inversion method to reproduce its inputs. Figure 1 shows an example of the correlation between the annual 1900-1990 climate indices predicted thru inversion of SWING model (the Melbourne University Global Climate Model- MUGCM) isotopes and the climate indices derived directly from the model output, versus the number of years used in 'training' the K matrix. We see in the figure that for training periods less than approximately 50 years, the inversion is unable to reproduce the 1900-1990 time series with strong correlations, but for 50 years or more training the correlation is approximately .5 or better for all of the indices. Similar correlations are found if the inputs are all empirical instead of model.

The utility in using the climate models is to develop a K matrix for climate regimes of the past. The first step toward that end is to model the recent, observed, climate to validate the relationships between the climate indices and the ice cores. Figure 2 shows a similar correlation to Figure 1, but for the

inversion of the actual ice core isotopes using the same K matrix as above, with the output indices correlated with the actual climate indices. Other than temperature, the correlation between the indices resulting from the inversion and the actual climate indices is low. Ongoing work will be performed with longer than annual averaging, which is expected to provide stronger relationships between the model isotopes and climate indices and will also be more consistent with the empirical data.

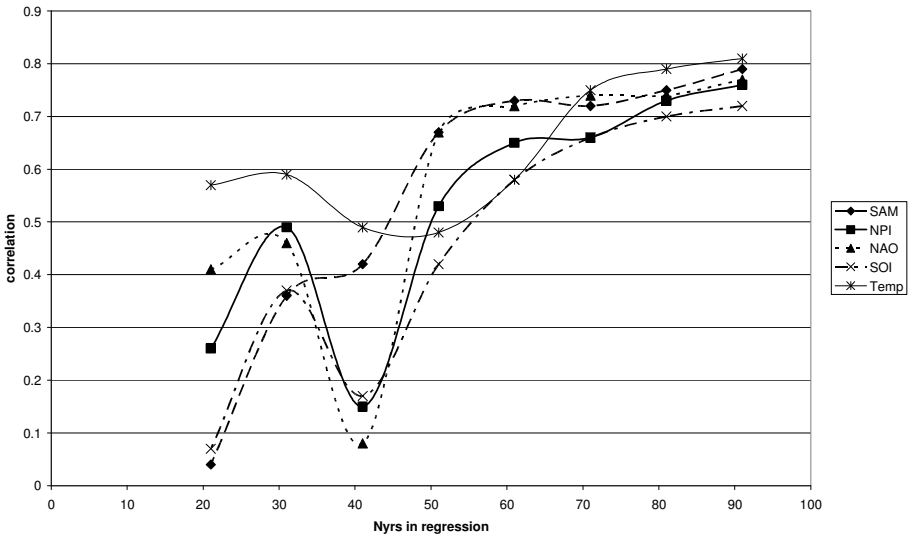

Figure 1: Correlation of the climate indices output from the inversion of the MUGCM derived ice cores' isotopes with the climate indices taken directly from the model outputs.

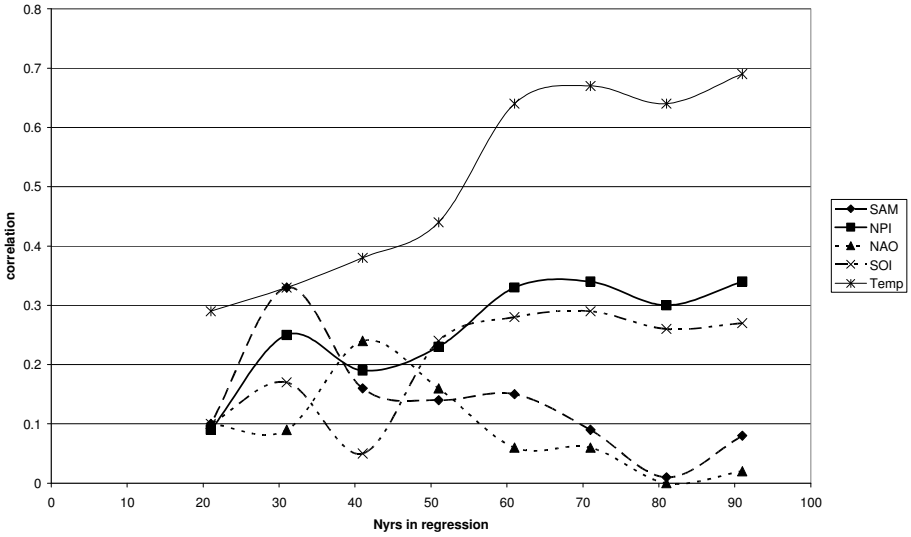

Figure 2: Correlation of the climate indices output from the inversion of the actual ice cores' isotopes with the empirical climate indices. The K matrix for the inversion is the same as in Figure 1.

Rodgers 2000. Inverse Methods for Atmospheric Sounding, Theory and Practice: World Scientific Publishing

Antarctic Peninsula warming from model simulations

Karpenko A.A., Mokhov I.I.
A.M. Obukhov Institute of Atmospheric Physics RAS, Moscow, Russia

Significant surface air temperature (SAT) increase has been observed during the last decades in the Southern Hemisphere over the Antarctic Peninsula (Turner and Pendlebury, 2004; Karpenko et al., 2005; Turner et al., 2005; Mokhov et al., 2006). In this paper, we analyze the ability of global climate models to simulate the observed tendency of warming near surface in the Antarctic Peninsula region with an assessment of possible temperature changes in the 21st century. In particular, simulations with general circulation models HadCM3 and HadGEM1 for the 4th IPCC Report (Climate Change, 2007) with the SRES-A1B and SRES-A2 scenarios are used as well as simulations the IAP RAS climate model (CM) of intermediate complexity.

Figure 1 shows the SAT changes (relative to 1961-1990) for the Bellingshausen station from model simulations in comparison with observations. The SAT increase from observations for this region is reproduced realistically by the models. General tendency of temperature increase for the 21st century from the model simulations is accompanied by remarkable variations, in particular in the first half of the century from HadGEM1 and HadCM3 simulations. The total SAT increase to the end of the 21st century relative to the end of 20th century according to model simulations for this region is estimated about 1.5 K for HadCM3, in the range 2-3 K for HadGEM1 and about 2.3-2.8 K for IAP RAS CM.

This work was partly supported by the programs of the Russian Academy of Sciences by the Russian Foundation for Basic Research.

References:

Climate Change 2007: The Physical Science Basis. Intergovernmental Panel on Climate Change. S. Solomon, D. Qin, M. Manning et al. (eds.). Cambridge Univ. Press. Cambridge, 2007. 1009 pp.

The International Antarctic Weather Forecasting Handbook. J. Turner and S. Pendlebury (eds.) British Antarctic Survey. Cambridge, 2004. 663 pp.

Karpenko, A.A., I.I. Mokhov, P.A., 2005: Contribution of natural and anthropogenic causes in regions with large temperature changes during XX century. Research Activities in Atmospheric and Oceanic Modelling. J. Cote (ed.), WMO TD-No.1276, Section 7, 9-10.

Turner, J., S.R. Colwell, G.J. Marshall, T.A. Lachlan-Cope, A.M. Carleton, P.D. Jones, V.E. Lagun, P.A. Reid, and S. Iagovkina, 2005: Antarctic climate change during the last 50 years. Intern. J. Climatol., 25, 279-294.

Mokhov, I.I., A.A. Karpenko, and P.A. Stott, 2006: Highest rates of regional climate warming over the last decades and assessment of the role of natural and anthropogenic factors. Doklady Earth Sci., 406, 1, 158–162.

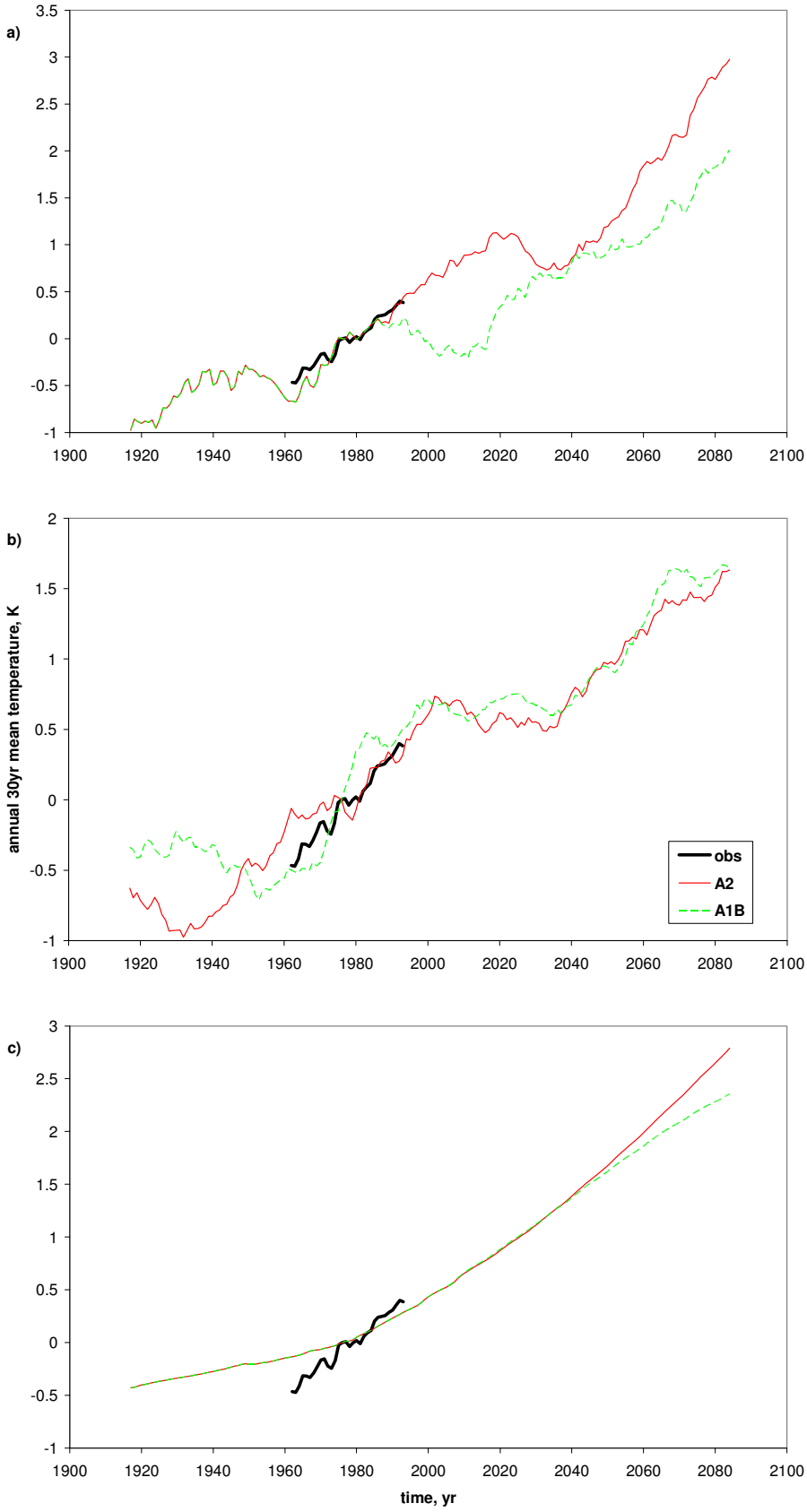

Figure 1. Changes of the SAT 30-year running means (K) for the Bellingshausen station region from observations and model simulations: a) HadGEM1, b) HadCM3, c) IAP RAS CM.

Nonlinear analysis of interaction between El Niño and Atlantic equatorial mode

S.S. Kozlenko[1, 3], I.I. Mokhov[1] and D.A.Smirnov[2]
[1]A.M. Obukhov Institute of Atmospheric Physics RAS, Moscow, Russia
[2]Saratov Branch, Institute of RadioEngineering and Electronics RAS, Russia
[3] Moscow Institute for Physics and Technology, Dolgoprudny, Russia
kozlenko@ifaran.ru

Based on the nonlinear techniques for the estimation of coupling between oscillatory systems, we analyze the interaction between equatorial Pacific mode (El Niño–Southern Oscillation or ENSO) and equatorial Atlantic mode (EAM).

We use several monthly mean indices for El Niño (EN) and EAM based on the HADISST data set (Rayner et al., 2003) for sea surface temperature (SST) since 1870 till 2006: Niño3 (5S-5N, 150W-90W) and Niño3.4 (5N-5S, 170W-120W) in the Pacific and Atlantic3 (20W-0, 3S-3N) in the Atlantic (see also (Keenlyside and Latif, 2007)).

Interaction between EN and EAM was studied with the use of cross-wavelet analyses in (Mokhov et al, 2007) where it was offered to use also methods based on phase dynamics modeling and nonlinear "Granger causality".

The quantitative characteristic of the cause-and-effect relationship introduced by Granger is defined as the prediction improvement (PI) of one signal when another signal (possibly, time delayed) is taken into account in the predictive model (Granger, 1969). The results of such analysis are compared to those obtained with cross-wavelet analysis and phase dynamic analysis.

Fig.1 demonstrates the prediction improvement and statistical significance level (estimated via F-test) versus trial time delay. Both with nonlinear Granger analysis and phase dynamic analysis, the presence of EAM → ENSO influence is detected. Thus, the conclusion about the presence of the EAM → ENSO influence is inferred at significance level $p < 0.0001$ (in other words, with confident probability greater than 0.9999) for a zero time delay (accuracy of time delay estimation is not greater than 1 month). Backward influence is not detected.

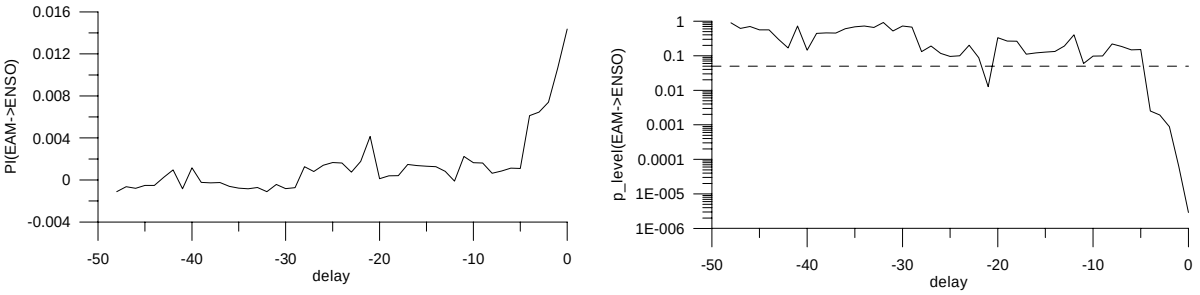

Fig.1. Estimation of the EAM → ENSO influence. Prediction improvement normalized by the ENSO variance (left panel) and statistical significance level (right panel) versus trial time delay between.

To reveal trends in coupling during the last decade, we estimate coupling between NAO and ENSO in a moving window of the length of 30 years. We started with the interval 1870–1900 and finished with 1975–2005. PI-values reveal increase in the strength of the influence EAM→ENSO (Fig.2).

Interaction between North Atlantic Oscillation (NAO) and ENSO has already been studied in (Mokhov, Smirnov, 2006). To get more complete picture of interactions between Atlantic and equatorial Pacific processes, we plan to investigate mutual dynamics of NAO and EAM in the same way.

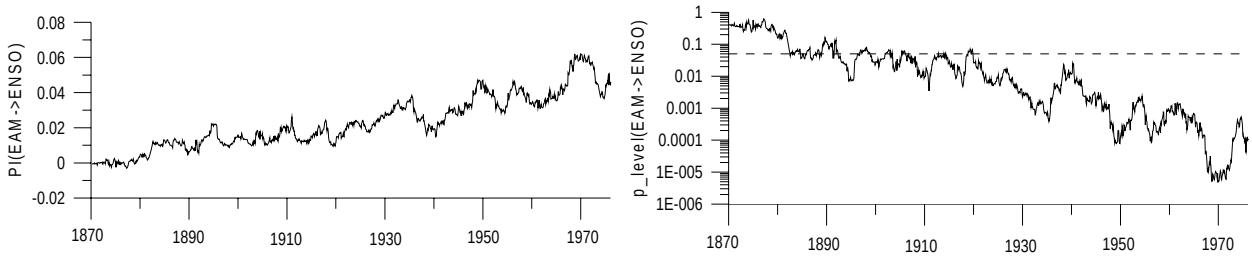

Fig.2. Influence EAM→ENSO (for zero trial time delay) in a 30-year moving window.

The work is supported by the Russian Foundation for Basic Research (grant No. 07-05-00381) and the RAS program.

References

Granger C.W.J. 1969. Investigating causal relations by econometric models and cross-spectral methods. *Econometrica*. V.37. P.424-438.

Keenlyside N.S., and Latif M., 2007: Understanding Equatorial Atlantic Interannual Variability. *J. Climate*, **20**, 131-142.

Mokhov I.I., Bezverkhny V.A., Karpenko A.A., Keenlyside N.S., Kozlenko S.S. 2007. Cross-wavelet analysis of coherence and time lags between El Nino and Atlantic equatorial mode. *Research Activities in Atmospheric and Oceanic Modelling*. Cote J. (ed.). Geneva: World Climate Research Programme. p.2.19-2.20.

Mokhov, I.I., and Smirnov D.A., 2006a: El Niño–Southern Oscillation drives North Atlantic Oscillation as revealed with nonlinear technique from climatic indices. *Geophys. Res. Lett.*, **33**, L03708, doi:10.1029/2005GL024557.

Rayner N.A, Parker D.E., Horton E.B., Folland C.K., Alexander L.V., Rowell D.P., Kent E.C. and Kaplan A., 2003: Global analyses of sea surface temperature, sea ice, and night marine air temperature since the late nineteenth century. *J. Geophys. Res*., 108 (D14), doi:10.1029/2002JD002670.

Zebiak, S.E., 1993: Air-sea interaction in the equatorial Atlantic region. *J. Climate*, **6**, 1567-1586.

Relationships between global surface temperature, carbon dioxide atmospheric content, solar and volcanic activity during the last 150 years

Igor I. Mokhov[1] and Dmitry A. Smirnov[2]

[1] *A.M. Obukhov Institute of Atmospheric Physics of Russian Academy of Sciences, Moscow, Russia; e-mail: mokhov@ifaran.ru*
[2] *Saratov Branch of the Institute of RadioEngineering and Electronics of Russian Academy of Sciences, Saratov, Russia; e-mail: smirnovda@info.sgu.ru, smirnovda@yandex.ru*

Global surface temperature (GST) has considerably increased during the last century [1,2]. Revealing the relative contribution of the natural and anthropogenic factors to the climate change is one of the key global problems [1,3]. The purpose of this work is to estimate relative influence of different factors including solar and volcanic activity and carbon dioxide (CO_2) atmospheric content on the GST changes from observational data with the aid of empirical bivariate and multivariate autoregressive (AR) models [4].

We analyzed the time series of GST anomalies during the last 150 years (1856-2005) [2]. Let us denote it $\{T(t)\}_{t=1856}^{2005}$. Solar activity $\{I(t)\}$ was represented by reconstruction [5]. Volcanic activity (1856-1999) is represented by the time series $\{V(t)\}$ of the stratospheric aerosol optical depth [6]. CO_2 concentration $\{n(t)\}$ in the atmosphere (1856-2004) is taken from [7].

First, we constructed an individual autoregressive (AR) model of GST variations in the form

$$T(t) = a_0 + a_1 T(t-1) + ... + a_d T(t-d) + \xi(t), \qquad (1)$$

where $\xi(t)$ is Gaussian white noise, coefficients a_j are estimated via the least-squares technique, the model order *d* is selected so to provide the least prediction error σ_ξ^2 maintaining "parsimonious" model. We found that the optimal order is *d* = 4 which provides noise variance $\sigma_\xi^2 = 0.01\,K^2$. The model AR-process appears stationary. It exhibits time series quite close to the observed one. However, the GST increase in 1985-2005 is not predicted by the model constructed from the interval 1856-1985 (Fig.1). It implies that something has changed in the external influences during the period 1985-2005.

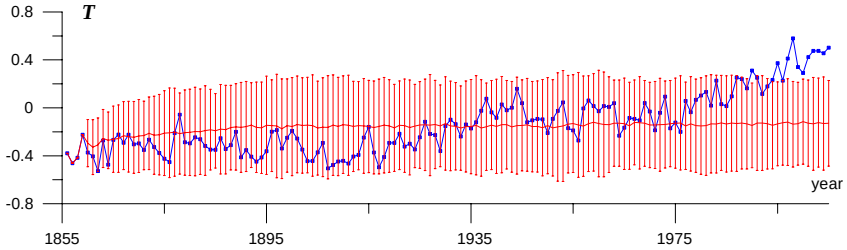

Figure 1: The observed time series of GST (in K) [2] (blue line) and an ensemble of time realizations of the model (1) of the order d = 4 constructed from the time interval 1856-1985. The ensemble is represented by its mean (red line) ± double standard deviation (error bars).

Relative value of the model prediction error for the period 1856-1985 is $\sigma_\xi^2 / \mathrm{var}[T] = 0.34$, i.e. one third of the GST empirical variance is attributed to the external influences. This part of GST variations can be to some extent explained by taking into account the other factors. If so, one infers the presence of the corresponding influences. This is the idea of the Granger causality estimation.

We constructed joint AR-models taking into account only one of the above three factors, or two of them, or all three of them. Influences of all three factors are detected. An optimal bivariate model accounting for the influence of solar activity has the form

$$T(t) = a_0 + a_1 T(t-1) + a_4 T(t-4) + b_I I(t-1) + \xi(t). \qquad (2)$$

E.g., if the data [5] for the period 1856-1985 is used for model fitting, then the solar variations influence is statistically significant at the significance level $p < 0.035$. However, the influence is not strong: the model (2) reduces the noise variance σ_ξ^2 only by 2.8 % as compared to the model (1). Thus, the model (2) gives somewhat better predictions than the model (1) but is not capable to predict GST increase in 1985-2005 as well.

A bivariate model accounting for the volcanic activity influence during the period 1856-1985 reduces σ_ξ^2 only by 1.2 % as compared to model (1) and does not predict the recent GST increase.

An optimal bivariate model accounting for the CO_2 concentration influence during 1856-1985 is

$$T(t) = a_0 + a_1 T(t-1) + a_4 T(t-4) + b_{1,n} n(t-1) + b_{2,n} n(t-2) + \xi(t)\,. \qquad (3)$$

It reduces σ_ξ^2 by 8.8 % and adequately predicts the GST increase in 1985-2005 (Fig.2). If constant value of CO_2 is used as the driving signal, the trend in GST is not observed.

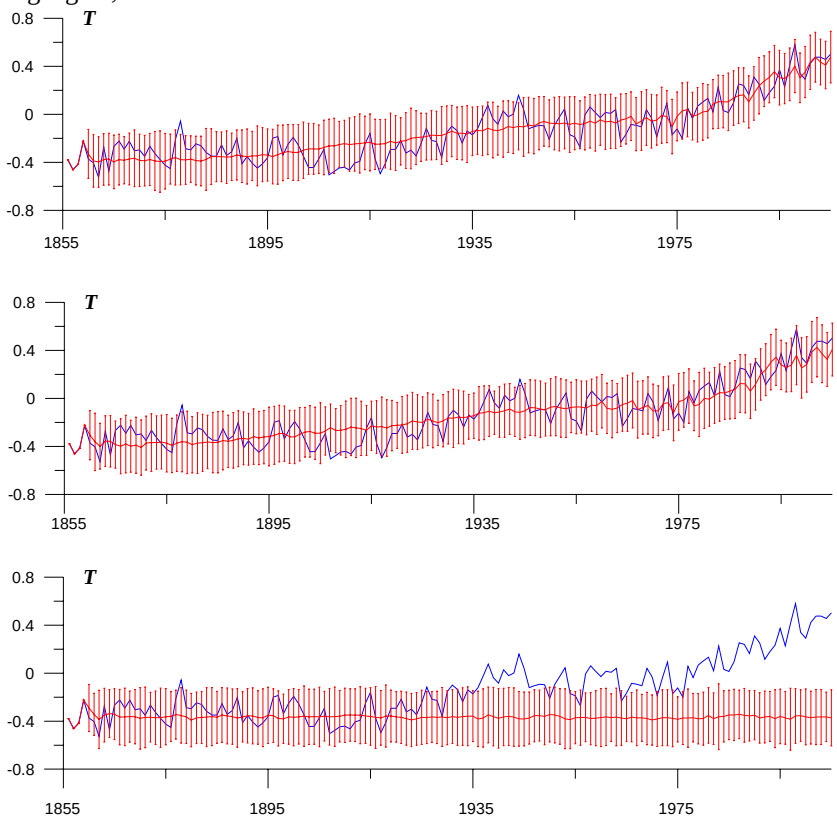

Figure 2: The observed time series of GST [2] (blue line) and ensembles of time realizations of the model (3) under different conditions. Upper panel: the model is constructed from the interval 1856-2005, the observed record of CO_2 (1856-2005) is used as a driving signal. Middle panel: the model is constructed from 1856-1985, the observed record of CO_2 (1856-2005) is used as a driving signal. Lower panel: the model is constructed from 1856-1985, constant CO_2 concentration (at the level of 1856) is used as a driving signal.

An optimal model with all factors has the form

$$T(t) = a_0 + a_1 T(t-1) + a_4 T(t-4) + b_I I(t-1) + b_{1,n} n(t-1) + b_{2,n} n(t-2) + b_V V(t) + \xi(t)\,, \qquad (4)$$

i.e. current value of GST depends on the previous-year solar activity, current-year volcanic activity, and CO_2 concentration for the two previous years. This joint model reduces the value of noise variance by 10 % as compared to the model (1). Such an improvement is highly statistically significant. About 8-9 % should be attributed to the CO_2 influence and only 1-2% to solar and volcanic activity together.

Nonlinear AR-models were also constructed. However, they involve more free parameters then linear models. The use of nonlinear models did not allow confident conclusions about coupling, most probably, due to the shortness of the available time series.

According to our analysis the most important anthropogenic factor (CO_2 concentration) determines the GST increase during last decades to a significant extent while the influence of solar and volcanic activity is by the order of magnitude weaker.

The work is supported by the Russian Foundation for Basic Research and programs of Russian Academy of Sciences.

1. Climate Change 2001: The Scientific Basis. Intergovernmental Panel on Climate Change, Ed. by J. Toughton, Y. Ding, D. J. Griggs, M. Noguer, et al. (Cambridge Univ. Press, Cambridge, 2001).
2. Climate Research Unit (University of East Anglia): http:// www.cru.uea.ac.uk
3. Mokhov I.I. et al. *Cosmic Research*. 2008. V.46. No.4.
4. Granger C.W.J. *J. Econ. Dynam. Control*. 1980. V.2. P.329-352.
5. Lean J. et al. *Solar Physics*. 2005. V.230. P.27–53.
6. Sato M. et al. *J. Geophys. Res*., 98, 22,987-22,994, 1993.
7. National Oceanic & Atmospheric Administration: http://www.esrl.noaa.gov/gmd/ccgg/trends/

WGNE Intercomparison of Tropical Cyclone Forecasts using Operational Global Models

Hirokatsu Onoda
Numerical Prediction Division, Japan Meteorological Agency
1-3-4 Otemachi, Chiyoda-ku, Tokyo 100-8122, JAPAN
(E-mail : h.onoda@met.kishou.go.jp)

1. Introduction

The CAS/JSC Working Group on Numerical Experimentation (WGNE) has conducted an intercomparison of Tropical Cyclone (TC) track forecasts using operational global models since 1991. WGNE recognized that the evaluation of TC track forecasts could revealingly indicate the performance of those models in the tropics and subtropics. As of in 2007, eleven NWP centers were contributing to this project.

2. Dataset

Table.1 shows the specification of the data provided by NWP centers, model resolutions and usage of TC bogus data in the analysis system. Table.2 gives a list of the responsible TC regional or warning centers providing analyzed TC position data (best track) for each basin.

Table.1 Specification of verification data provided by NWP centers

NWP center (Country)	Since	Horizontal resolution of provided data	Model resolution	TC bogus
JMA (Japan)	1991	1.25x1.25	T_L319 L40	Use *1
ECMWF (Europe)	1991	0.25x0.25	T_L799 L91	-
Met Office (UK)	1991	0.38x0.56	0.38x0.56 L50	Use
CMC (Canada)	1994	1.0x1.0	0.9x0.9 L28	-
DWD (Germany)	2000	0.5x0.5	40km L40	-
BoM (Australia)	2003	0.75x0.75	T_L239 L33	-
NCEP (USA)	2003	1.0x1.0	T_L382 L64	Use *2
Météo France	2004	0.5x0.5	T_L359 C1 L41	Use *3
CMA (China)	2004	Not GPV data	T213 L41	-
NRL (USA)	2006	1.0x1.0	T239 L30	Use
CPTEC (Brazil)	2006	0.9376x0.9376	T126 L28	-

*1: used in western North Pacific
*2: used in rare cases
*3: used except south Pacific and North Indian Ocean

Table.2 Best-track data

Region	Data source
western North Pacific	RSMC-Tokyo
eastern North Pacific	RSMC-Miami
Central Pacific	RSMC-Miami
North Atlantic	RSMC-Miami
North Indian	RSMC-New Delhi
South Indian	RSMC-La Reunion
around Australia	TCWC-Perth/Darwin /Brisbane/Wellington and RSMC-Nadi

RSMC : Regional Specialized Meteorological Centre
TCWC : Tropical Cyclone Warning Centre

3.Verification

The same verification method as Sakai and Yamaguchi (2005) is adopted in this study. The performance of TC track forecasts is evaluated by position errors and detection rates.
The detection rate(T) is defined as A(T)/B(T). (T = forecast time), where

A : The number of forecast events in which a TC is analyzed at forecast time T on the condition that a NWP model continuously expresses the TC until the forecast time T.

B : The number of forecast events in which a TC is analyzed at forecast time T.

Systematic position errors are also monitored after being stratified (categorized) by stage with respect to recurvature : before, during and after recurvature.
The verification is conducted for each of the six regions where TCs are analyzed under the WMO Tropical Cyclone Programme. In this paper, the results for the western North Pacific, North Atlantic and around Australia regions with inhomogeneous sample (the number of track points is different in each NWP center) are shown.

4.Result for the western North Pacific region

The time series position error for 72-hour forecast from 1991 to 2006 are shown in Fig1(a). Fig1(b) indicates the position error growth and Fig1(c) does the detection rate descent as forecast time progresses in 2006. Fig2 shows the scattering diagram of position error for 72-hour forecast. The Y-axis represents the position error for Along Track (AT) direction and the X-axis does for Cross Track (CT) direction.

5.Results for North Atlantic and around Australia regions

Fig3 and Fig4 show the verification results of position error and detection rate for North Atlantic and around Australia regions, respectively.

Reference
Tsuyuki, T. et al., 2002: The WGNE intercomparison of typhoon track forecasts from operational global models for 1991-2000. WMO-BULLETIN, vol.5, No.3, 253-257.
Sakai, R., and M. Yamaguchi, 2005: The WGNE Intercomparison of Tropical Cyclone Track Forecasts by Operational Global Models. CAS/JSC WGNE Research Activities in Atmospheric and Oceanic Modeling, Report No. 35, Jul 2005, WMO/TD No.1276, pp. 2.7-2.8.

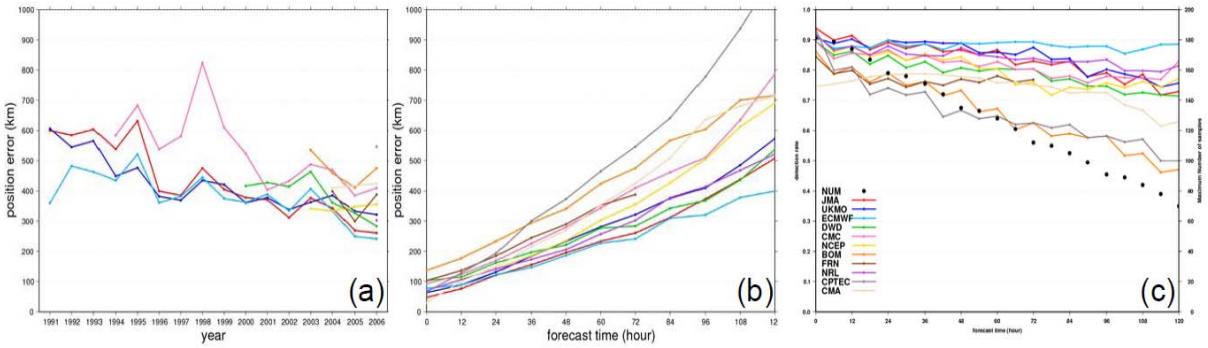

Fig.1 (a) Time series of position error for 72 hour forecast in western North Pacific (1991-2006). (b) Position error growth in western North Pacific in 2006. (c) Detection rate descent in western North Pacific in 2006.

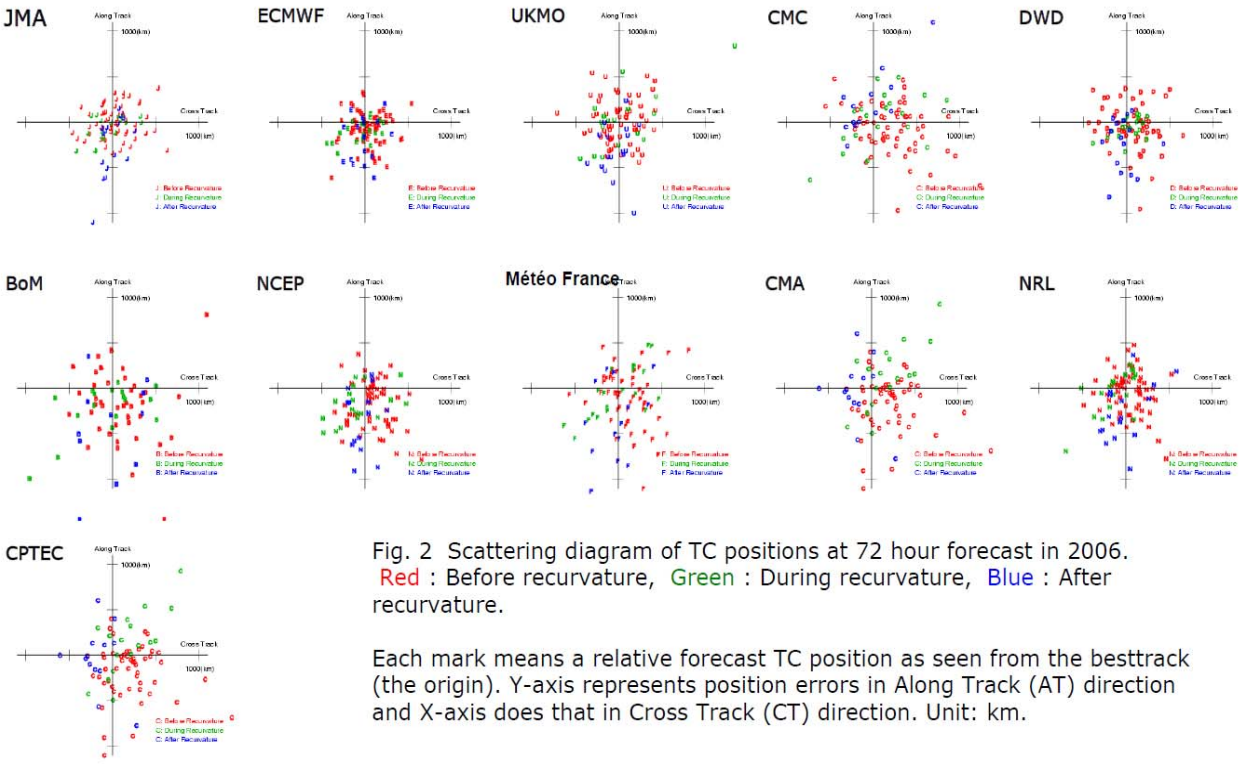

Fig. 2 Scattering diagram of TC positions at 72 hour forecast in 2006.
Red : Before recurvature, Green : During recurvature, Blue : After recurvature.

Each mark means a relative forecast TC position as seen from the besttrack (the origin). Y-axis represents position errors in Along Track (AT) direction and X-axis does that in Cross Track (CT) direction. Unit: km.

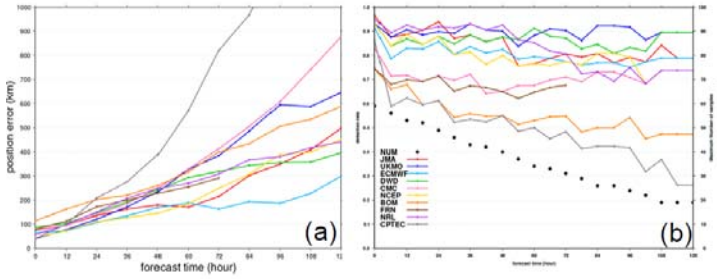

Fig.3 :North Atlantic region in 2006
(a) Position error
(b) Detection rate
Legend is the same as Fig.1.

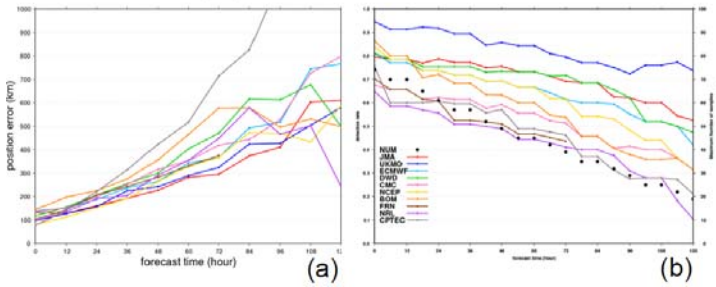

Fig.4 :around Australia region in 2006
(a) Position error
(b) Detection rate
Legend is the same as Fig.1.

THE HYDRODYNAMIC- STATISTICAL MODEL OF OPERATIVE FORECAST OF THE COMPLEX OF DANGEROUS PHENOMENA (HEAVY RAINFALL, STORM WIND INCLUDING SQUALL AND TORNADO, THUNDERSTORM AND HAIL) AT THE TERRITORY OF RUSSIA

E.V.Perekhodtseva

(Hydrometeorological Center of Russia, B.Predtechenskii 9-13, 123242, Moscow, Russia, e-mail: perekhodtseva@rhmc.mecom.ru)

Development of successful method of forecast of strong summer winds, including squalls and tornadoes, heavy rainfall, thunderstorm and hail could allow to take the proper of the measures against destruction of buildings and other damage. Well-in-advance successful forecast (from 12 hours to 36 hour) makes possible to reduce the losses. Prediction of these phenomena is a very difficult problem for synoptic till recently. The existing graphic and calculation methods still depend on subjective decision of an operator.

At the present time in Russia there is no hydrodynamic model for forecast of the maximal speed of summer wind over then 20m/c and 25m/c, of the maximal quantity of precipitation more than 20mm/12h, of the thunderstorm and the hail. Hence the main tools of objective forecast of such phenomena are statistical methods using the dependence of the phenomena involved on a number of atmospheric parameters (predictors).

The statistical decisive rules of the alternative and probability forecast of these events were obtained in accordance with the concept of "perfect prognosis" using the data of objective analysis. For this purpose the teaching samples of the present and of the absent of these phenomena were automatically arranged that include the values of forty physically substantiated potential predictors.

The choosing of the group of slightly connected and informative predictors for every phenomenon was done by the empirical statistical method [1]. This method uses the diagonalization of the mean correlation matrix **R** of the predictors for every phenomenon and the extraction of diagonal blocks of strongly correlated predictors. Thus for every of foregoing phenomenon the most informative predictors were selected without loosing of information. Those predictors include either a representative of each block or some of independent informative predictor. We obtained for every phenomenon corresponding the group of the most informative predictors or the vector-predictor (we used the criterion of distance of Mahalanobis and criterion of minimum of entropy by Vapnik-Chervonenkis [1]). The statistical decisive rules for diagnosis and prognosis of every phenomenon were calculated for this vector-predictor. The development of the operative non-adiabatic hydrodynamic model for short-term forecast (the author – Berkovich L.V.) and improvement of 36h forecasts of pressure, temperature and others parameters allow us to use the prognostic fields of those models for the calculation of the values of the discriminant functions

and of the probabilities for prognosis either of dangerous wind or the precipitation or the thunderstorm or the hail in the nodes of the greed 150x150km and thus to get fully automated forecasts of these phenomena. At the map of European part of Russia the prognosis area of the forecast of foregoing phenomenon obtains by extraction of the isoline of the probability with empiric threshold **P.** This threshold of the probability was obtained for every phenomenon.

According to the Pirsey-Obukhov criterion (T), the success of these hydrodynamic - statistical methods of forecast of squalls and tornadoes to 36 hours ahead for the warm season , was used at the regional Departments of Meteorology likes Central Region, the Region of High Volga (Nizhnii Novgorod), at the North-West Region (St-Petersburg) and others Regions as the automated objective calculation method, is T = 0,54-0,78 [2,4]. The forecast of the heavy precipitation with the quantity over 15mm/12h and over 50mm/12h are after the independent tests successful too. The criterion of Pirsy-Obukhov was 0.52-0.76 [4]. The alternative forecast of present of the thunderstorm and the hail has high enough assessment too. Such assessments were also obtained for the forecast of storm wind and heavy rainfalls at territory of Siberia during 2003-2005 years [3,4].

This way the synoptic can to take all of the maps of the forecast to 12-36h ahead for the every of foregoing phenomena together and then to extract the areas with three prognostic events (the storm wind, including squall and tornado, the heavy rainfall, the thunderstorm or the hail). These prognostic fields of appear probabilities of these phenomena calculated two times a day into operative system of Hydrometeorological Center of Russia. This automated method enables to use the forecast to 12h, 24h and 36h ahead of the complex of dangerous phenomena in the operative practice at the Departments of Meteorology of Russia.

REFERENCES

1) Perekhodtseva E.V. The forecast of the squalls on the basis of the diagnostic and prognostic connections. The proceedings of the Hydrometcenter of the USSR, 1985, issue 271, pp. 37-60.
2) Perekhodtseva E.V The model of automated forecast of dangerous and hazard wind including squalls and tornadoes for the territory of Europe. EGU – 2006, Vienna, April
3) Perekhodtseva E.V Hydrodynamic - statistical model of operative forecast to 12-36h ahead of storm winds including squalls and tornadoes at the territory of Siberia. 2006. Research activities in atmospheric and oceanic modeling. Rep.48
4) Perekhodtseva E.V The hydrodynamic-statistical model of the forecast of the catastrophic phenomena like squalls, tornadoes, floods, landslides and mudflows. International conference “Analysis and Singularity”. Moscow, Russia, August 21 – 25, 2007.

‘Energy box diagram’ investigation of South Atlantic hurricane Catarina

Alexandre Bernardes Pezza, José Augusto Paixão Veiga*, Ian Simmonds and Pedro Leite da Silva Dias**

School of Earth Sciences, The University of Melbourne, Victoria 3010, Australia

*Centro de Previsão de Tempo e Estudos Climáticos, Instituto Nacional de Pesquisas Espaciais, São José dos Campos, São Paulo, Brazil.

**University of São Paulo, São Paulo, Brazil

e-mail: apezza@unimelb.edu.au

The unusual cyclone Catarina (2004) in Brazil has earned a place in history as the first observed South Atlantic hurricane during the satellite era. It originated as a baroclinic (frontal) cyclone, undergoing Tropical Transition (TT) and achieving hurricane status while still keeping a hybrid structure (Pezza and Simmonds, 2005). The partition into zonal and eddy components of both the atmospheric Available Potential Energy (AZ and AE, respectively) and Kinetic Energy (KZ and KE, respectively) as proposed by Lorenz (1967) is here adopted to study the energetics associated with the transition of this very rare event. As far as we are aware this is the first time that such technique is used to study a TT case in the Southern Hemipshere. The cycle is completed by the conversion between the various energy forms given by CA (from AZ to AE), CE (from AE to KE), CK (from KE to KZ), and CZ (from AZ to KZ). Here the Lorenz diagram is presented so that the conversion terms are always positive and the arrows indicate the direction of the fluxes (figure 1a). For more details on the methodology the reader is referred to Wahab et al. (2002) and references therein.

Figure 1b shows the day of greater baroclinic conversion (March 21, 12 UTC) when Catarina was still driven by the westerlies and clearly frontal. For that particular time the term CE was dominant, meaning that the eddy kinetic energy KE was growing at the expense of the available energy in a highly baroclinic way. The conversion term CA indicates that the energy flow discussed above was originating from the zonal available potential energy AZ, and the barotropic conversion term CK shows only a small contribution towards increasing the zonal kinetic energy. The sudden transition of Catarina is seen in figure 1c for March 22nd at 06UTC. The diagram for that particular time shows a significant change in the energy cycle with the

baroclinic conversion terms CE and CA becoming very small and the barotropic conversion CK becoming the major driver. The time series of the baroclinic conversion terms CE and CA (figure 1d) indicated a sharp maximum on the 21st followed by an increase in CK (negative) on the following day, with the other terms presenting less pronounced changes. A likely mechanism for the reduction in the baroclinicity was the formation of the blocking system over the domain, cutting Catarina off from the westerlies.

Lorenz, E. N., (1967), The Nature and Theory of the General Circulation of the Atmosphere. World Meteorological Organization, 161 pp.

Pezza, A.B., and Simmonds, I, 2005: The first South Atlantic hurricane: Unprecedented blocking, low shear and climate change. *Geophysical Res. Letters,* **32**, doi:10.1029/2005GL023390.

Wahab M. A., Basset, H. A. and Lasheen A. M. (2002), On the mechanism of winter cyclogenesis in relation to vertical axis tilt. *Meteorol. Atmos. Phys.*, 81, 103-127.

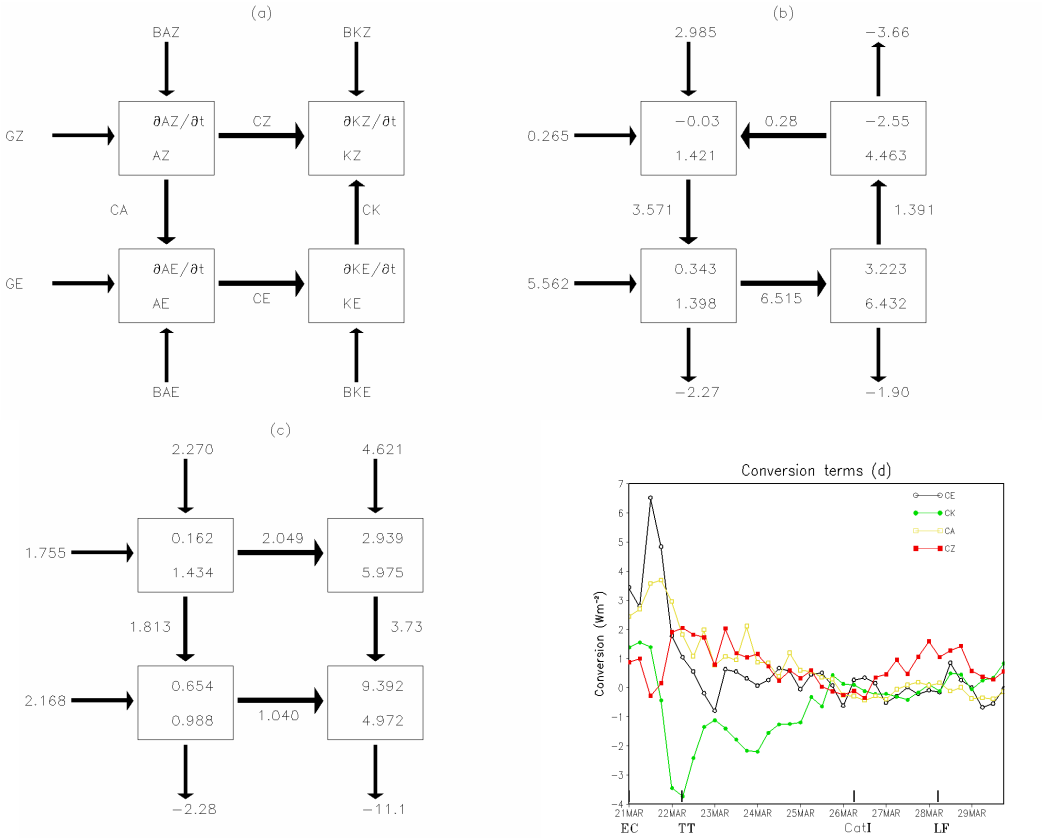

Figure 1: Volume integrated energy terms for (b) 2112 UTC and (c) 2206 UTC. Panel (d) shows the time series of vertically integrated conversion terms (CA, CE, CK and CZ) for the period 21-29 March 2004. The relevant periods during Catarina's lifecycle are indicated in panel (d). Panel (a) shows the energy cycle here adopted as a reference guide. Units are in 10^5 J/m^2 and W/m^2, respectively, for energy and conversion terms. See text for further details.

Frontal features over the Southern Ocean

Ian Simmonds

School of Earth Sciences
The University of Melbourne
Victoria, 3010, Australia
simmonds@unimelb.edu.au

Cyclonic systems are intimately tied up with the maintenance of climate. There are now a number of sophisticated objective identification and tracking schemes which can be applied to analyses and model output (e.g., Simmonds and Keay 2000, Simmonds et al. 2003, Lim and Simmonds 2007) to diagnose all the relevant characteristics of these features. The automated identification of *frontal* structures is a much more difficult problem. While algorithms have been proposed (e.g., Hewson 1998, Kašpar 2003) these tend to work best when high resolution quality analyses are available. There is clearly a need for *complementary* frontal identification schemes which can be used when data quality is an issue.

We here show some experimental results obtained using a 'single point' approach with ERA-40 for 8 December 2001 18UTC. In Fig. 1 mobile fronts are identified over the southern Indian Ocean sector using a simple Eulerian **thermal** criteria. In the Figure grid points at which the 1000 hPa temperature decreases by more that 2ºC in 6 hours (i.e., for which dT (6 hrs) < -2ºC) are indicated by a '1' and blue colouring. Points for which dT (12 hrs) < -4ºC are indicated by a '2' and dark green colouring. Points at which both these criteria are satisfied are denoted by a '3' and light green colouring. In an analagous fashion Fig. 2 displays the result for the same synoptic case when a simple **dynamic** criteria is used. Those points for which the surface wind direction changes over 6 hours from the NW to the SW quadrant are indicated by '1' (blue colouring). At each of those identified points if the change in the *meridional* component of the wind exceeds 2 ms^{-1} the point is now indicated by '2' (dark green). The points which are flagged when this criterion is increased to 4 ms^{-1} and 6 ms^{-1} are marked with '3' (light green) and '4' (very light green), respectively. These basic experiments indicate that mobile frontal structures may be identified by rather simple algorithms.

Our present work is addressing the extent to which a combination of simple Eulerian criteria based on thermal, dynamic and other considerations can be of value in identifying these important frontal features.

Hewson, T. D., 1998: Objective fronts. *Meteor. Appl.*, **5**, 37-65.

Kašpar, M., 2003: Objective frontal analysis techniques applied to extreme/non-extreme precipitation events. *Studia Geophysica et Geodaetica*, **47**, 605-631.

Lim, E.-P., and I. Simmonds, 2007: Southern Hemisphere winter extratropical cyclone characteristics and vertical organizaton observed with the ERA-40 reanalysis data in 1979-2001. *J. Climate*, **20**, 2675-2690.

Simmonds, I., and K. Keay, 2000: Mean Southern Hemisphere extratropical cyclone behavior in the 40-year NCEP-NCAR reanalysis. *J. Climate*, **13**, 873-885.

Simmonds, I., K. Keay and E.-P. Lim, 2003: Synoptic activity in the seas around Antarctica. *Mon. Wea. Rev.*, **131**, 272-288.

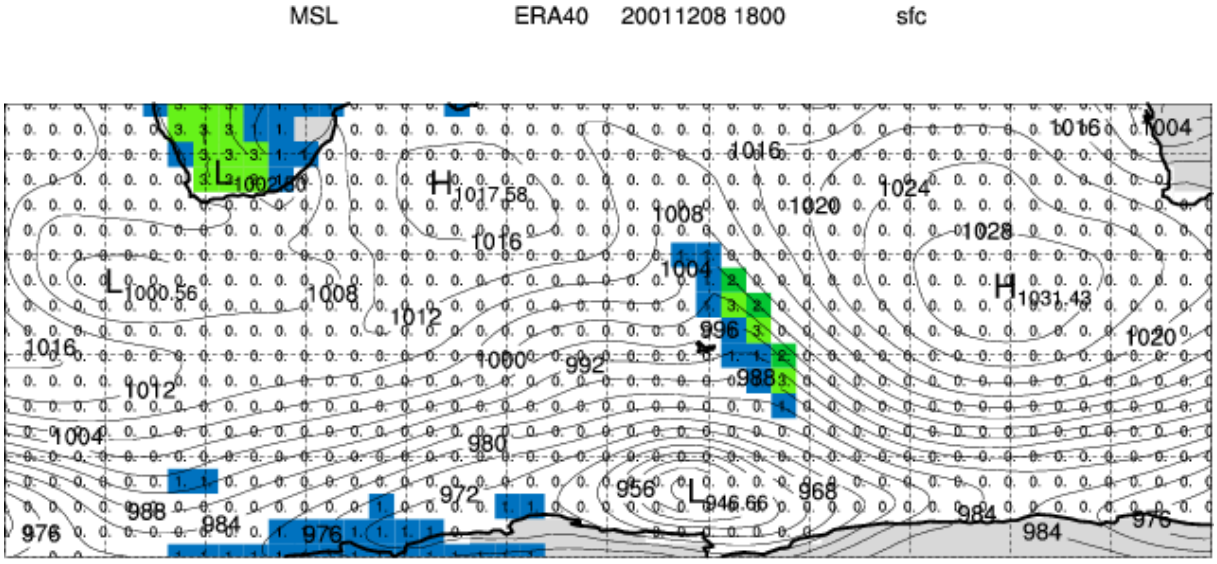

Figure 1: The fronts identified over the southern Indian Ocean sector on 8 December 2001 (18UTC) when using simple thermal criteria. Grid points at which the 1000 hPa temperature decreases by more that 2ºC in 6 hours (i.e., for which dT (6 hrs) < -2ºC) are indicated by a '1' and blue colouring. Points for which dT (12 hrs) < -4ºC are indicated by a '2' and dark green colouring. Points at which both these criteria are satisfied are denoted by a '3' and light green colouring.

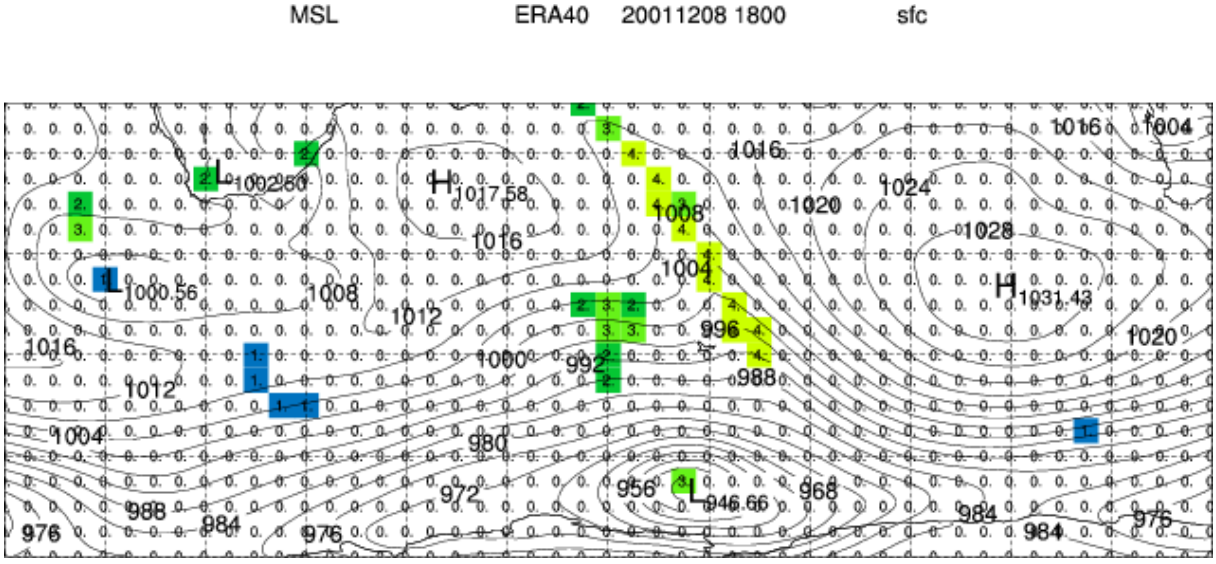

Figure 2: Fronts identified for the same case as in Figure 1, but using simple dynamic criteria. Those points for which the surface wind direction changes over 6 hours from the NW to the SW quadrants are indicated by '1' (blue colouring). All of these points for which, in addition, the change in the *meridional* component of the wind exceeds 2 ms^{-1} are indicated by '2' (dark green). The points which are flagged when this threshold is increased to 4 ms^{-1} and to 6 ms^{-1} are marked with '3' (light green) and '4' (very light green), respectively.